Passage rates of propagating interfaces in randomly advected media and heterogeneous media

Alan R. Kerstein and Wm. T. Ashurst
Combustion Research Facility, Sandia National Laboratories, Livermore, California 94551-0969
(Received 6 December 1993; revised manuscript received 22 March 1994)

The mean passage rate of a propagating interface, subject to random advection or random variation of the local propagation speed, is investigated analytically and computationally. A model representing the longitudinal propagation of two points of the interface separated by a fixed transverse distance is formulated and analyzed. In the limit of weak random perturbations, the model predicts several parameter dependences of the mean passage rate. These predictions are evaluated by performing two-dimensional and three-dimensional numerical simulations of interface propagation. The analysis addresses broadband (i.e., multiscale, as in turbulent flow) as well as narrow-band perturbations. In the broadband case, scaling laws governing transient as well as statistically steady propagation are derived. The numerical simulations span a sufficient range of perturbation amplitudes to exhibit the complete amplitude dependence of the mean passage rate, including scaling behaviors governing the weak and strong perturbation limits.

PACS number(s): 05.40.+j, 02.50.−r, 43.30.+m, 47.70.Fw

I. INTRODUCTION

Passage-rate problems associated with propagation phenomena arise in diverse contexts, including applications in which the front is a physical interface and others in which the front is a mathematical construct describing a statistical property of an evolution process. The latter applications are exemplified by models of the growth and geographical spread of animal populations [1]. In applications of this type, the instantaneous state of the system is determined by the spatial locations of all members of the population. The notion of front propagation arises in this context from consideration of the time evolution of isopleths (i.e., level sets) of a coarse-grained instantaneous number density, or alternatively, the time evolution of an ensemble-average density profile.

For problems in which the front is defined by coarse graining or ensemble averaging, details of the instantaneous spatial structure are suppressed and the questions of greatest interest concern the time evolution of the front. Typically, the process is described by a partial differential equation governing the evolution of the spatial profile of number density [1]. If there exists a steadily propagating solution, then the corresponding velocity eigenvalues represent the mean rate of population spread, or in the terminology used here, the mean passage rate. There is extensive literature concerning both the mathematical aspects of the eigenvalue analysis and its diverse physical applications [1,2].

The problems considered here involve Huygens-type propagation of fronts that are physical interfaces. Again, the physical applications are diverse, ranging from phase change (e.g., solidification) and deposition processes to chemical (e.g., combustion) and physical (e.g., optical or acoustic) impulses traversing advected or spatially heterogeneous media. Owing to the interesting structural features of such interfaces, studies to date have focused primarily on their geometrical scaling properties [3].

Progress toward the solution of passage-rate problems for interface propagation processes has been limited. A paradigm of the passage-rate problem for heterogeneous media is the first-passage percolation problem [4], related to the geometrical concept of chemical distance (shortest allowed path) [5]. First-passage percolation has been analyzed and simulated numerically for lattices composed of bonds randomly designated as open (propagation rate unity) or blocked (propagation rate zero). Rigorous analysis has focused on demonstrating the existence of the passage rate and the equivalence of various definitions of the passage rate. Exact determination of the passage rate is deemed to be mathematically intractable [6].

Passage-rate problems fall broadly within the class of problems concerning the determination of effective properties of random media from the microstructure [7]. Various analytical methods have been developed for the investigation of problems of this type, in particular, variational methods for determining bounds on effective properties [8]. It has not yet been demonstrated that these methods are useful for analyzing passage-rate problems. The approach adopted here has no obvious antecedent in the literature on effective properties of random media.

Recent work by the present authors identified a scaling governing passage-rate problems for a class of interface propagation processes [9]. Scaling analysis, confirmed computationally, was used to show that the mean passage rate of propagating interfaces subject to weak random advection increases in proportion to the $\frac{4}{3}$ power of the amplitude of the random perturbations. The mechanism underlying this scaling was shown to involve an intermediate time scale, here denoted τ_d, longer than the time for the interface to propagate across one correlation length of the flow, but shorter than the flow correlation time. τ_d is the time scale over which a balance

between interface wrinkling and smoothing processes is established. These results were obtained by applying a form of dimensional analysis [10] to a variant of the Kardar-Parisi-Zhang (KPZ) equation governing stochastic interface growth [11].

Here a discrete analog of continuum propagation is formulated and analyzed in order to gain further understanding of the weak perturbation regime. The discrete analog is a model of the time evolution of two points of the interface whose transverse separation is of the order of the flow correlation length. The growth of interface height at these points is governed by two stochastic differential equations whose coupling reflects the geometry governing the propagation of curved interfaces.

Analysis and numerical simulation of spatially discrete models is one of the principal techniques that has been used to study the structural features of propagating interfaces [12]. The discrete model formulated here is used to study parameter dependences of the passage rate. Lattice problems previously considered in the context of first-passage percolation are not kinematically equivalent to continuum propagation in the weak-advection limit. The desired equivalence is achieved here by transverse discretization, with a continuum representation of longitudinal evolution.

The analysis treats propagation in advected media and in spatially heterogeneous media within a common framework. In the limit of weak random perturbations (reflecting either weak advection or small variations of the local propagation speed), these two problems are shown to be formally equivalent. The analysis identifies the roles of the three distinct time scales governing the propagation process and provides clarification of the mechanisms determining the passage rate.

In the weak perturbation regime, the discrete model is amenable to systematic analysis and its interpretation as an analog of continuum propagation, though nonrigorous, is plausible. Beyond this regime, an artifact of the model renders it invalid for quantitative analysis. To validate the model in the weak perturbation regime and to determine parameter dependences of the passage rate beyond this regime, numerical simulations of continuum propagation in advected media and in spatially heterogeneous media are performed. The simulations are the first to span a sufficient range of perturbation amplitudes to exhibit the complete dependence of the passage rate on perturbation amplitude and are thus of intrinsic interest apart from their use for model validation.

The discrete model, denoted the "two-point model," reproduces the previously derived $\frac{4}{3}$-power dependence of the mean passage rate on perturbation amplitude. Moreover, it predicts a $\frac{2}{3}$-power dependence of the passage rate on the ratio of characteristic length scales of the perturbing field and the propagating interface. This result is useful to the extent that the ratio can be characterized in a simple manner. For the class of perturbing fields employed in the simulations, the ratio is found to depend only on spatial dimension. This result indicates the possibility that the coefficient in the relation between the mean passage rate and perturbation amplitude depends on spatial dimension, but not on other details of the perturbing field. Additional parametric studies would be required to determine the generality of this simplest of possible outcomes.

A scaling technique is used to extend the analysis to propagation in self-similar flows. Scaling laws are derived for steady and transient propagation regimes in such flows.

This paper is organized as follows. In Sec. II, the propagation processes considered here are specified and physical applications are noted. In Sec. III, the two-point propagation model is formulated and analyzed. In Sec. IV, predictions are compared to computer simulation results. In Sec. V, propagation subject to self-similar perturbations is analyzed.

II. INTERFACE PROPAGATION PROCESSES

The most general formulation of interface propagation that is considered here is represented by the "flame propagation" equation [9,13]

$$\frac{\partial h}{\partial t} + \mathbf{v}_\perp \cdot \nabla h = u[1 + (\nabla h)^2]^{1/2} + v_\parallel . \tag{1}$$

Here $h(\mathbf{x},t)$ is the interface height as a function of transverse location $\mathbf{x}$ and ∇ is the gradient with respect to $\mathbf{x}$. h is taken to be a single-valued function of $\mathbf{x}$. This is strictly valid only in the weak perturbation limit, owing to the occurrence of overhangs at finite perturbation amplitude. [To maintain formal generality, the expansion of the square root in powers of $(\nabla h)^2$, yielding the nonlinear term of the KPZ equation [11], is not implemented at this stage.]

The interface $h(\mathbf{x},t)$ is subject to (i) advection by a given flow field $\mathbf{v}(\mathbf{x},h,t)$ whose longitudinal and transverse components are denoted $v_\parallel$ and $\mathbf{v}_\perp$, respectively, and (ii) normal propagation at speed $u(\mathbf{x},h,t) = \lambda + V(\mathbf{x},h,t)$, consisting of the mean speed λ plus a fluctuating part V. The notation reflects an analogy between the two sources of fluctuations, the flow field $\mathbf{v}$ and the propagation speed fluctuation V. Namely, if the amplitudes of these fluctuating quantities are taken to be small, then expansion of Eq. (1) to leading order in $\mathbf{v}$, V, and $(\nabla h)^2$ gives

$$\frac{\partial h}{\partial t} = \lambda + \frac{\lambda}{2}(\nabla h)^2 + V + v_\parallel , \tag{2}$$

showing the formal equivalence of V and $v_\parallel$ in this regime. (The smallness of the omitted term $\mathbf{v}_\perp \cdot \nabla h$ relative to terms that are retained is discussed in Ref. [9] and in Sec. III B.)

The physical implication of Eqs. (1) and (2) is that propagation in randomly advected media and propagation in media that are heterogeneous in the sense that u is spatially varying (allowing also an autonomous time

variation) are equivalent processes in the small-amplitude limit, but may differ qualitatively at finite perturbation amplitudes. Many physical applications involve both types of fluctuations. Flame fronts in turbulent flow are subject to local flame speed fluctuations caused by strain and flame curvature [13]. Acoustic impulses propagating through the ocean are subject to local sound speed fluctuations caused by temperature and pressure variations and to advection by currents and eddies. In practice, advection is the dominant effect in turbulent combustion and heterogeneity is the dominant effect in oceanic sound propagation [14], so these applications may be regarded as examples of the respective propagation processes. Another example of propagation through a heterogeneous medium is combustion of solid composite propellants [15].

In the acoustics literature, the formulation analogous to Eq. (2) is the stochastic Helmholtz equation. This formulation and an equivalent ray-tracing formulation are discussed by Karweit *et al.* [16]. They cite the literature in which the approximations leading to these formulations are developed. Analogous considerations in the combustion literature are discussed by Williams [13]. For the present purposes, Eq. (1) is adopted as a generic paradigm, yielding Eq. (2) in the weak perturbation limit.

A feature that distinguishes Eq. (1) from the KPZ equation is the dependence of the fluctuation terms on spatial location, parametrized by $(\mathbf{x}, h)$, as well as on time. It has been noted that the dependence of the fluctuations on h introduces nonlinear couplings that complicate efforts to apply analytical methods developed for the case of autonomous fluctuations [10]. Here Eq. (1) is analyzed for the case of autonomous fluctuations as well as for the case of h-dependent fluctuations in order to show that the former is not merely a special case of the latter. The two cases are shown to exhibit qualitatively different behaviors.

The distinction between these cases is highlighted because the physical applications considered here correspond to the more difficult and less widely studied case of location-dependent fluctuations. The location dependence is self-evident for a heterogeneous medium whose spatial variation of u is regarded as a specified property of the medium. For an advected medium, $\mathbf{v}(\mathbf{x}, h, t)$ is determined by an evolution equation, typically the Navier-Stokes equation. For present purposes, $\mathbf{v}$ is treated as a random field with specified properties.

A further complication arising in some physical applications is the effect of the propagation process on the perturbing fields u and $\mathbf{v}$. In turbulent combustion, heat release at the interface causes thermal expansion that affects the evolution of $\mathbf{v}$. In fluid or solid combustion, the transport processes that determine u locally may depend on front curvature and thus on higher derivatives of h [13]. The diverse nonlinear couplings that arise in various applications cause the parametric dependences of the mean passage rate to be problem specific. Complications of this nature are omitted here in order to maintain focus on the effect of specified location-dependent fluctuations, with no feedback from the propagation process to the processes determining u and $\mathbf{v}$.

III. TWO-POINT MODEL

A. Model formulation

A discrete analog of continuum propagation is formulated in order to achieve an analytically tractable representation that captures the underlying physical mechanisms and reproduces the parameter dependences of the continuum process. For clarity, the model is formulated with reference to an advected interface with constant propagation speed $u = \lambda$. The advection process $\mathbf{v}(\mathbf{x}, h, t)$ is taken to be a narrow-band vector field characterized by a correlation length L, defined explicitly in Sec. III B. (Generalization to broadband advection is considered in Sec. V.)

The discrete model is interpreted in terms of continuum propagation based on an idealized representation of interface geometry. For illustration, propagation in a two-dimensional medium is considered. The interface at any instant is represented by a collection of circular arcs, as illustrated in Fig. 1. This geometry is an idealization of Huygens-type propagation of advected interfaces. Constant-speed propagation (without advection) starting from an arbitrary initial interface causes the interface to evolve to a collection of circular arcs [11]. Advection causes the arcs to deviate from circular shape.

A "two-point" advection-propagation model is formulated to represent the evolution of interface height $h(x_{1,2}, t)$ at two transverse locations x_1 and x_2. Adopting the notations $h_{1,2}(t) = h(x_{1,2}, t)$, $h_+ = \max(h_1, h_2)$, and $h_- = \min(h_1, h_2)$, and denoting the perturbations at $x_{1,2}$ by $v_{1,2}$ (with $v_\pm$ defined accordingly), the model consists of two coupled evolution equations

$$\frac{\partial h_+}{\partial t} = \lambda + v_+, \tag{3}$$

$$\frac{\partial h_-}{\partial t} = \lambda \left[1 + (\nabla h_-)^2\right]^{1/2} + v_-. \tag{4}$$

Here $v_\pm$ is the model analog of $v_\parallel$. As in the continuum formulation, $v_\pm$ depends in general on t and on spatial location parametrized by $(x_\pm, h_\pm)$, where x_+ and x_- are the transverse locations corresponding to h_+ and h_-, respectively (e.g., $x_+ = x_1$ and $x_- = x_2$ if $h_1 > h_2$). ∇h_- represents the gradient of h evaluated at x_-.

This formulation is related to Fig. 1 by interpreting x_- as the transverse location of an end point and x_+

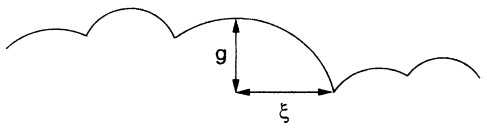

FIG. 1. Idealized representation of the instantaneous geometry of a propagating interface in two dimensions. The characteristic interface length scale ξ is represented here as the transverse separation of adjacent extrema. The longitudinal separation of the extrema is denoted g.

as the transverse location of the maximum of a typical arc of that figure. At the maximum, $\nabla h = 0$, hence the absence of a ∇h contribution from Eq. (3). Based on the geometry of Fig. 1, ∇h at an end point is $2\xi|g|/(\xi^2 - g^2)$, where $g = h_2 - h_1$ and $\xi = |x_2 - x_1|$. Specializing to the weak perturbation limit, $\nabla h_- = 2g/\xi$ to leading order in $g/\xi \ll 1$. The notation $\nabla h_- = cg/\xi$ is adopted, where $c = 2$ for the geometry of Fig. 1. (The value of c is immaterial in what follows because c is subsumed into an empirical coefficient.)

In the weak perturbation limit, Eq. (4) can be approximated by

$$\frac{\partial h_-}{\partial t} = \lambda + \frac{\lambda}{2}(\nabla h_-)^2 + v_-, \tag{5}$$

indicating the equivalence of this formulation to Eq. (2). Subtraction of Eq. (5) from Eq. (3) and substitution of the approximate expression for ∇h_- gives

$$\frac{\partial g}{\partial t} = -\frac{\lambda c^2}{2\xi^2} g|g| + w, \tag{6}$$

where $w = v_2 - v_1$. For now, w is treated as random process depending only on time, so that Eq. (6) determines the statistics of g in terms of the properties of $w(t)$. Consequences of the dependence of $v_{1,2}$, and thus of w, on $x_{1,2}$ and $h_{1,2}$ will be considered presently.

For either sign of g, the term that is nonlinear in g causes g to approach zero, consistent with the physical picture that the propagation process causes smoothing of interfaces and, in particular, reduces the curvature of the circular arcs of Fig. 1. Equation (6) also indicates that the transverse gradient of longitudinal velocity, here represented in discretized form by w, is the source of fluctuations of g, consistent with previous analysis of continuum propagation [9]. Thus, Eq. (6) embodies the mechanisms reflected in Eq. (2), with the advantage that key properties of g are readily analyzed.

Equations (3) and (5) can be ensemble averaged to obtain $\langle \partial h_+/\partial t \rangle = \lambda + \langle v_+ \rangle$ and $\langle \partial h_-/\partial t \rangle = \lambda + (\lambda c^2/2)\langle (g/\xi)^2 \rangle + \langle v_- \rangle$. Due to invariance under exchange of labels 1 and 2,

$$\left\langle \frac{\partial h_1}{\partial t} \right\rangle = \left\langle \frac{\partial h_2}{\partial t} \right\rangle = \frac{1}{2}\left(\left\langle \frac{\partial h_+}{\partial t} \right\rangle + \left\langle \frac{\partial h_-}{\partial t} \right\rangle \right)$$
$$= \lambda + \frac{\lambda c^2}{4}\left\langle \left(\frac{g}{\xi}\right)^2 \right\rangle + \langle v_1 \rangle . \tag{7}$$

This quantity is interpreted as the model analog of the mean passage rate u_T of a continuum interface. (The notation is motivated by the "turbulent flame speed" in combustion applications.) This interpretation is strictly valid if the transverse locations of the maxima and end points of the arcs in the continuum geometry of Fig. 1 are constant in time. Because this is not the case, a given transverse location will on occasion correspond to an arc maximum or end point, but in general will be neither. The rate of longitudinal advance of the interface, averaged over the transverse coordinate(s), need not equal the rate of advance averaged only over arc maxima and endpoints.

Nevertheless, the proposed interpretation should give the correct scalings of u_T, based on the following consideration. For an interface in a spatial continuum, u_T is equal to λ times the surface area of the interface per unit projected transverse area because the volume swept by the interface is proportional to its surface area [13]. For the geometrical picture of Fig. 1, the analogous quantity for a given transverse segment ξ is λ times the arc length within the segment divided by ξ. To leading order in $g/\xi \ll 1$, the length-to-span ratio is $1 + \frac{2}{3}(g/\xi)^2$ for given g and ξ. Averaging over segments, with each segment weighted by its span ξ, gives

$$\frac{u_T}{\lambda} = 1 + \frac{A}{\langle \xi \rangle}\left\langle \frac{g^2}{\xi} \right\rangle, \tag{8}$$

where $A = \frac{2}{3}$. Because the geometrical picture of Fig. 1 is qualitative at best, A is regarded as an undetermined coefficient.

Implicit in the derivation of Eq. (8) is the assumption that there is no mean flow in the longitudinal direction, corresponding to vanishing of the spatial average of v_1. This does not imply that the term $\langle v_1 \rangle$ in Eq. (7) vanishes, because that term is equivalent to a time average of v_1 evaluated at the instantaneous interface location $h_1(t)$. The propagation process induces correlations between h_1 and v_1, so $\langle v_1 \rangle$ does not vanish, but it is shown in Sec. III B that it is negligible in the weak perturbation limit. Anticipating that result, $\langle v_1 \rangle$ is henceforth omitted from the analysis.

Equations (7) and (8) imply equivalent scalings provided that fluctuations of ξ are governed by a single characteristic length scale. Letting ξ now denote a characteristic interface length scale, Eqs. (7) and (8) can be expressed generically as

$$\frac{u_T}{\lambda} = 1 + A\frac{\langle g^2 \rangle}{\xi^2}. \tag{9}$$

The differing mechanistic origins of Eqs. (7) and (8) are thus subsumed into the coefficient A.

There are several simplifications inherent in the characterization of interface geometry by a single length scale. Spatial and temporal variations of the local interface length scale are neglected, as are details of the kinematic couplings among the arcs portrayed in Fig. 1. As noted earlier, the representation of the interface as a collection of circular arcs is also a simplification.

The justification of these simplifications is ultimately empirical. In Sec. III B, a mean-passage-rate expression is derived that involves the ratio L/ξ, where L is a characteristic length scale of the perturbing field. If passage rates measured or simulated in diverse circumstances can be correlated based on a simple assumption concerning this ratio, then the present picture is operationally useful, if not mechanistically confirmed. Numerical simulations are interpreted from this viewpoint in Sec. IV.

The connection between the two-point model and continuum propagation in three dimensions is not readily

expressed in terms of a geometrical picture analogous to Fig. 1. In the weak perturbation regime, the scaling $u_T/\lambda - 1 \sim \langle(\nabla h)^2\rangle$ is valid in three as well as two dimensions, so Eq. (9) should still be applicable. The operational definition of ξ is now ambiguous, but the choice of definition should only affect the value of the coefficient A.

In Eq. (9), $\langle g^2\rangle$ denotes the variance of g determined from Eq. (6) for statistically steady propagation. The transient dependence of u_T can be analyzed by treating $\langle g^2\rangle$ in Eq. (9) as an ensemble average at given t and treating Eq. (6) as a stochastic initial-value problem for given statistics of $g(0)$. Here the principal focus is the large-t limit, corresponding to statistically steady propagation. For statistically steady propagation, Eqs. (6) and (9) determine u_T in terms of λ and the statistics of the fluctuating quantity w. Some aspects of transient propagation are considered in Sec. V.

The key feature of Eq. (6) is its quadratic dependence on g, analogous to the quadratic nonlinearity in Eq. (2). The origin of the nonlinearity is geometrical, arising from the projection of the propagation vector, locally normal to the interface, onto the longitudinal coordinate corresponding to the height variable h [11]. The present analysis provides an explicit demonstration of the effect of the nonlinearity on the parameter dependences of u_T.

B. Analysis of the weak perturbation limit

Solution of Eq. (6) is straightforward if $w(t)$ is a white noise. Self-consistent reasoning is used to show that $w(t)$ is effectively a white noise in the weak perturbation limit. Namely, the white noise property is assumed, the steady-state value of $\langle g^2\rangle$ is estimated, and the estimate is used to validate the white noise assumption.

Assuming white noise, Eq. (6) is a Langevin equation with nonlinear dissipation. The fluctuation term induces growth of g^2 whose rate can be estimated from $dg^2/dt \sim D$, where D is the diffusivity of the random process $w(t)$. According to Eq. (6), decay of g^2 due to the dissipation term is of the form $dg^2/dt = -K|g^3|$, where K is of order λ/ξ^2. Growth and decay are in balance when $K|g^3| = D$, giving $\langle g^2\rangle \sim (D/K)^{2/3}$. This determines a decay time scale τ_d by expressing the decay term $Kg|g|$ in Eq. (6) in the form g/τ_d, giving $\tau_d \sim K^{-1}\langle g^2\rangle^{-1/2} \sim (K^2D)^{-1/3}$, or

$$\tau_d \sim (\lambda^2 D/\xi^4)^{-1/3}. \tag{10}$$

The diffusivity D and the correlation time τ_w of the random process $w(t)$ are analyzed, providing a comparison of τ_w and τ_d and thus a self-consistent test of the white noise assumption. D is determined by the relation [17]

$$D = \int_0^\infty \langle w(0)w(t)\rangle\, dt. \tag{11}$$

Recalling that $w = v_2 - v_1$, the consequences of the dependences of the quantities $v_{1,2}$ on $x_{1,2}$ and $h_{1,2}$ are now considered. w is written in the form $w = v_2(h_2(t),t) - v_1(h_1(t),t)$, indicating both the explicit dependence on t and the implicit dependence through $h_{1,2}$. The dependence on $x_{1,2}$ is implied by the subscript notation and therefore is not shown as an argument of $v_{1,2}$. Substitution of this expression for w into Eq. (11) yields four terms. Invoking spatial homogeneity, the interchange of subscripts reduces the result to

$$D = 2\int_0^\infty \langle v_1(h_1(0),0)v_1(h_1(t),t)\rangle\, dt - 2\int_0^\infty \langle v_1(h_1(0),0)v_2(h_2(t),t)\rangle\, dt. \tag{12}$$

To proceed further, additional properties of v_1 and v_2 must be specified. v_1 and v_2 are determined by evaluating a continuum field $v_\parallel(x,h,t)$ at $(x_1,h_1(t),t)$ and $(x_2,h_2(t),t)$, respectively. Here $v_\parallel$ is the longitudinal (h) component of a homogeneous, isotropic, statistically steady random flow field $\mathbf{v}$. Denoting the variance of $\mathbf{v}$ as v'^2, isotropy implies $\left\langle v_\parallel^2\right\rangle = v'^2/d$ for d-dimensional flow, where the angular brackets now denote an average over d-dimensional space. (For clarity, the analysis is limited to $d = 2$, but generalization to other d is straightforward.) Accordingly, $v_{1,2}'^2 = v'^2/d$, where $v_{1,2}'^2 \equiv \langle v_{1,2}^2\rangle$. The correlation length and time of v_1, defined as [18]

$$L = \langle v_1^2\rangle^{-1}\int_0^\infty \langle v_1(0,0)v_1(h,0)\rangle\, dh \tag{13}$$

and

$$\tau_v = \langle v_1^2\rangle^{-1}\int_0^\infty \langle v_1(0,0)v_1(0,t)\rangle\, dt, \tag{14}$$

respectively, correspond to the correlation length and time of $v_\parallel$.

With these definitions, the weak perturbation limit can now be formally defined as the limit of small v'/λ (in the spatial continuum) or small v_1'/λ (in the two-point model). To evaluate D in the weak perturbation limit for given v_1', L, and τ_v, $h_{1,2}(t)$ is approximated by λt in Eq. (12). This can be justified self-consistently by noting that $dh_{1,2}/dt$ is governed at any instant by either Eq. (3) or (5). Provided that $|\nabla h_-|$ is small (which follows from the ensuing analysis, hence the self-consistency), the right-hand side of either equation is λ plus terms much smaller than λ. Denote the magnitude of the additional terms as M. Neglect of the additional terms is valid provided that the resulting error in, say, $h_1(t)$ is much less than the distance L over which v_1 varies significantly. The error for given t is of order Mt. The error is therefore determined by the range of t over which the integrands of Eq. (12) are non-negligible.

The integrands are correlations of quantities displaced both in time and in space. The correlations are negligible if the temporal displacement is much greater than the correlation time τ_v or if the spatial displacement is much greater than the correlation length L. The latter condition is more restrictive. Because $h_{1,2}(t)$ is approximately λt, the latter condition implies that the relevant range

of t is of order L/λ. This is smaller than τ_v because the ratio $\tau_v/(L/\lambda)$ is of order λ/v_1' (based on the dimensional relation $v' \sim L/\tau_v$), which is much greater than unity in the weak perturbation limit.

Thus the integrands of Eq. (12) are non-negligible for t of order L/λ, giving an error of order ML/λ. This is much smaller than L, as required to justify the approximation for $h_{1,2}(t)$, provided that $M \ll \lambda$. According to Eqs. (3) and (5), this condition is satisfied provided that $|\nabla h_-|$ is small, which is verified shortly.

The time scale L/λ, distinct from the flow correlation time τ_v, arises because the propagation process causes the interface to sweep past flow structures at a rate λ that greatly exceeds the rate of evolution v' of the structures. In the reference frame of the interface, the perturbations represented by the random process w have an effective correlation time $\tau_w = L/\lambda \ll \tau_v$ due to this rapid sweeping of the flow.

Sweeping effects are typically encountered in flow analysis in the context of the sweeping of small eddies by large eddies in turbulent flow. In that context, the sweeping effect is a complication largely responsible for the difficulty of turbulent flow analysis [19]. Here the sweeping effect simplifies the analysis of the weak perturbation limit, though away from this limit it is a complicating factor. The simplification arises because the effect is deterministic in this limit, governed by the constant propagation speed λ.

The upshot of these considerations is that $h_{1,2}(t)$ can be approximated by λt in Eq. (12) and, moreover, the explicit dependence on t (i.e., the second argument of $v_{1,2}$) is negligible. In other words, the flow is effectively frozen because the sweeping time is much shorter than the time for the flow to evolve. Equation (12) therefore gives

$$D = 2\int_0^\infty \langle v_1(0,0)v_1(\lambda t,0)\rangle\, dt - 2\int_0^\infty \langle v_1(0,0)v_2(\lambda t,0)\rangle\, dt. \tag{15}$$

With the change of variables $t = h/\lambda$, the first integral is found to be proportional to the flow correlation length L given by Eq. (13), so Eq. (15) reduces to

$$D = \frac{2\langle v_1^2\rangle L}{\lambda} - \frac{2}{\lambda}\int_0^\infty \langle v_1(0,0)v_2(h,0)\rangle\, dh. \tag{16}$$

The integrals in Eq. (15) differ in that the correlation function in the rightmost integral involves points displaced transversely by $\xi = x_2 - x_1$ as well as longitudinally by h. The leftmost integral therefore dominates provided that ξ is at least of order L, the length scale governing the falloff of velocity correlations with increasing displacement. It has been noted that interface fluctuations are generated at length scale L and that they are dissipated most effectively at small scales [as shown in Ref. [9] based on Eq. (2)], so the interface length scale ξ is indeed order L or larger. Therefore it is reasonable to neglect the rightmost term of Eq. (16), obtaining the simple relation

$$D = \frac{2\langle v_1^2\rangle L}{\lambda}. \tag{17}$$

This result reflects the role of the sweeping time scale $\tau_w = L/\lambda$. The diffusivity scales as V^2T, where V is a characteristic fluctuation amplitude and T is a characteristic time scale. Because V is of order v_1, Eq. (17) implies that T is of order τ_w, consistent with the physical processes underlying the properties of $w(t)$.

With this estimate of D, the parameter dependences of the passage-rate increment $(u_T/\lambda) - 1$ given by Eq. (9) can be obtained. Recalling [above Eq. (10)] that $\langle g^2\rangle \sim (D\xi^2/\lambda)^{2/3}$, Eq. (9) gives

$$\frac{u_T}{\lambda} - 1 \sim \left(\frac{L}{\xi}\right)^{2/3}\left(\frac{v'}{\lambda}\right)^{4/3}. \tag{18}$$

The analysis recovers the $\frac{4}{3}$-power dependence of the passage-rate increment on the ratio of the root-mean-square velocity fluctuation v' to the propagation speed λ, previously deduced from Eq. (2) based on dimensional considerations [9]. In addition, a factor involving the correlation length ratio L/ξ is obtained. ξ is not a known input because it is determined by the interaction of the advection and propagation processes. As noted in Sec. III A, the operational utility of this formulation is contingent on the determination of a simple relationship between ξ and L. In Sec. IV, evidence is presented in support of the proposal that L/ξ depends only on spatial dimension for some classes of perturbing fields.

In the weak perturbation limit, three distinct time scales governing advected propagating interfaces have been identified. The flow correlation time τ_v, of order L/v', is the slowest of the three. It has no direct relation to interface evolution mechanisms. The fast time scale $\tau_w \sim L/\lambda \sim (v'/\lambda)\tau_v$ characterizes advective perturbations in the reference frame of the interface. The relation $\tau_w \ll \tau_v$ allowed simplification of Eq. (12) for D, leading finally to Eq. (17). Substitution of Eq. (17) into Eq. (10) gives

$$\tau_d \sim (\xi/L)^{4/3}(v'/\lambda)^{1/3}\tau_v, \tag{19}$$

indicating that the time scale τ_d governing the smoothing effect of the propagation process is intermediate between τ_w and τ_v.

The relation $\tau_w \ll \tau_d$ validates the assumption that $w(t)$ in Eq. (6) is effectively a white noise relative to the time scale governing the propagation term and thus validates the diffusion picture leading to the derivation of Eq. (17). The estimate of τ_d also provides a rationale for the omission of the term $\mathbf{v}_\perp \cdot \nabla h$ from the left-hand side of Eq. (2). For isotropic flow, the time scale governing fluctuations of $\mathbf{v}_\perp$ in the reference frame of the interface is the same as the time scale τ_w governing longitudinal fluctuations. In an elapsed time τ_w, the transverse displacement of the interface is of order $v'\tau_w \sim (v'/\lambda)L$. Because L is of order ξ, this is much less than ξ, so the time required for a significant (i.e., order ξ) transverse displacement is much greater than τ_w. The diffusion picture is therefore applicable to transverse fluctuations. The time required for an order-ξ transverse displacement is estimated as

$\xi^2/D \sim (\xi/L)^2(\lambda/v')\tau_v$, which is much greater than the time scale τ_d governing the decay of fluctuations. This confirms the irrelevance of transverse displacements in the weak perturbation limit.

Because transverse fluctuations of the propagating interface are generated at length scale L by the flow, any interface fluctuations at transverse length scales larger than L must be generated by the $\mathbf{v}_\perp \cdot \nabla h$ term acting on size-L fluctuations. The slowness of this process relative to the decay process ensures that such fluctuations are not significant and therefore that ξ/L is not large. In conjunction with the earlier observation that ξ is at least of order L, this establishes that ξ/L is of order unity.

According to Eq. (9), the right-hand side of Eq. (18) is of order $(\nabla h_-)^2$. Because ξ/L is of order unity and v'/λ is small by assumption, Eq. (18) implies that $|\nabla h_-|$ is small, providing the required self-consistent verification of the assumption at the outset of the analysis.

The sweeping effect plays a key role in the foregoing analysis. An additional consequence of this effect is that the term $\langle v_1 \rangle$ in Eq. (7) is negligible in the weak perturbation limit, as claimed in Sec. III A. This is demonstrated self-consistently based on

$$h_1(t) = \lambda t + \int_0^t \delta(t')\, dt', \tag{20}$$

where $\delta(t) \equiv dh_1/dt - \lambda$. Taylor expansion of $v_1(h_1)$ gives

$$v_1(h_1) = v_1(\lambda t) + \left[\int_0^t \delta(t')\, dt'\right] \left.\frac{dv_1}{dh}\right|_{h=\lambda t} + \cdots . \tag{21}$$

Due to the assumed flow properties [below Eq. (12)], the ensemble average of $v_1(\lambda t)$ is zero. To estimate the average of the next term, note that relevant time scale t is the relaxation time τ_d. Also note that dv_1/dh is of order v'/L. Therefore $\langle v_1 \rangle$ is of order $\langle \delta \rangle \tau_d v'/L$. Based on the definition of δ, Eq. (7) is equivalent to $\langle \partial h_1/\partial t \rangle = \lambda + \langle \delta \rangle$. Therefore the contribution of $\langle v_1 \rangle$ is negligible provided that $\langle \delta \rangle \tau_d v'/L \ll \langle \delta \rangle$, which reduces to $\tau_d \ll \tau_v$. This inequality has been demonstrated, confirming that $\langle v_1 \rangle$ is negligible.

The scaling properties of interest, in particular Eq. (18), are thus established. The formal solution of Eq. (6) is now obtained in order to identify which aspects of the analysis are exact within the framework of model assumptions and which involve additional approximations. The probability density function $P(g;t)$ of $g(t)$ governed by the Langevin equation $\partial_t g = -F(g) + w$, where w is a white noise with diffusivity D, evolves according to the Fokker-Planck equation [20]

$$\partial_t P = \partial_g(FP) + D\partial_g^2 P. \tag{22}$$

For the special case $F(g) = Bg|g|$, where B is a numerical coefficient, this equation has been used [21] to obtain the steady-state variance $\langle g^2 \rangle = (3D/B)^{2/3}/\Gamma\left(\frac{1}{3}\right)$. Substitution of this result, with B corresponding to the coefficient of $g|g|$ in Eq. (6), into Eq. (9) gives

$$\frac{u_T}{\lambda} - 1 = \frac{A}{\Gamma(1/3)} \left(\frac{6D}{c^2 \xi \lambda}\right)^{2/3} \tag{23}$$

This result is expressed in terms of parameters of the advection-propagation process by substituting the approximate expression for D, Eq. (17), giving

$$\frac{u_T}{\lambda} - 1 = \frac{A}{d^{2/3}} \left(\frac{L}{\xi}\right)^{2/3} \left(\frac{v'}{\lambda}\right)^{4/3} . \tag{24}$$

Here numerical coefficients are subsumed into the parameter A. Though the ratio L/ξ is treated in practice as an empirical coefficient, it is retained explicitly for comparison to another case, considered next.

Namely, the case of autonomous perturbations is considered. Autonomous perturbations are characterized by an amplitude v' and a correlation time τ_v. The perturbations are not explicitly associated with a spatial structure. In particular, the relation $v' \sim L/\tau_v$ is no longer meaningful. A restricted class of flows can be formulated that reduces to the autonomous case in the weak perturbation limit. The exemplar flows considered in Sec. IV are of this type.

In this case, there is no time scale shorter than τ_v governing fluctuations of w. Dimensional estimation of D based on Eq. (12) therefore gives $D \sim v'^2 \tau_v$. Substitution into Eq. (23) gives

$$\frac{u_T}{\lambda} - 1 \sim \left(\frac{v'\tau_v}{\xi}\right)^{2/3} \left(\frac{v'}{\lambda}\right)^{2/3} . \tag{25}$$

The contrast between this result and the $\frac{4}{3}$-power dependence on v'/λ in Eq. (24) reflects the difference between autonomous perturbations and perturbations that depend on spatial location. The sweeping effect arises only in the latter case. The passage-rate scalings indicated in Eq. (25) may be applicable to physical processes that can be represented by Eq. (2) with autonomous random forcing [11]. Equation (25) should be interpreted with care because v' appears in both factors on the right-hand side. This point is considered further in Sec. IV.

Efforts to extend the analysis of advected propagating interfaces to finite-amplitude perturbations encounter serious difficulties. The two-point model as formulated is analyzed in the strong perturbation limit as readily as in the weak perturbation limit. In fact, Eq. (6) is replaced by an equation linear in g in this limit. The difficulty is that simplifications inherent in the model render it inapplicable to continuum flow in this limit. The model accounts for advection-induced tilting of the interface due to transverse variation of the longitudinal flow velocity $v_\parallel$, but it omits the contribution of the transverse advection term of Eq. (1). At finite amplitude, transverse advection becomes significant and introduces complications such as overhangs, i.e., multiple valuedness of $h(\mathbf{x}, t)$. Likewise, the $\langle v_1 \rangle$ term in Eq. (7) becomes significant and its evaluation is problematic.

Studies of the strong perturbation limit based on scaling and similarity analysis have been performed [13,22–25]. Dimensional considerations indicate that u_T is proportional to v' in this limit, because the process is advection dominated and the only available, dimensionally correct parameter group is v' itself. The two-point model does not recover this result, giving instead

$u_T \sim (\lambda v')^{1/2}$, which is readily obtained by analyzing this limit using the methods of Sec. III A. This result is an artifact of the anisotropy implicit in the occurrence of large g values with no allowance for overhangs. In the weak perturbation limit, the anisotropy of the two-point model is physically correct, reflecting the near planarity of the interface. (Lattice models necessarily involve strong local deviations from planarity, hence the continuum representation of the longitudinal coordinate in the two-point model.) In the strong perturbation limit, the two-dimensional continuum picture implied by the two-point model involves replacement of the circular arcs of Fig. 1 by vertically stretched elliptical arcs, a far different picture from the isotropic structure expected under conditions of advection dominance.

IV. COMPARISON TO NUMERICAL RESULTS

A. Formulation of an exemplar class of perturbing fields

An exemplar class of perturbing fields is formulated for the purpose of investigating numerically the parameter dependences of u_T, both within and beyond the regime of validity of the two-point model. The computations span a range of v'/λ sufficient to determine the scaling behaviors in the strong as well as the weak perturbation limit. The formulation encompasses the two types of perturbation identified in Sec. II: constant-speed propagation of randomly advected interfaces and variable-speed interface propagation in a fixed heterogeneous medium.

The choice of perturbing field is constrained by computational feasibility. There are distinct considerations in the limits of small and large v'/λ. For small v'/λ, the characteristic time governing interface area growth is much greater than the time for the interface to sweep forward one correlation length (as shown in Sec. III B). Therefore numerical simulation requires propagation of a longitudinal distance of many correlation lengths to achieve relaxation of initial transients. It is impractical to construct and store a velocity field of the required size prior to the simulation. Rather the perturbation field ahead of the interface is constructed on an ongoing basis. A class of perturbing fields that can be constructed in this manner was formulated in a previous numerical study of the weak perturbation regime [9].

That class of perturbing fields does not, however, satisfy the computational requirements for large v'/λ. The front-tracking technique that is efficient for small v'/λ [9] becomes impractical due to its inability to handle the overhangs and multiple connectedness that occur for large v'/λ. In this regime, it is advantageous to employ the field-equation technique, in which the evolving interface is represented as an isosurface of a scalar field $G(\mathbf{x},t)$ that is governed by a nonlinear evolution equation [26]. This approach requires the field G to obey periodic boundary conditions in transverse directions and a jump-periodic boundary condition in the longitudinal direction.

The computational method adopted here is to apply the front-tracking technique at small v'/λ and the field-equation technique at large v'/λ, thereby obtaining u_T over the desired range. The method is applied to a class of perturbing fields that satisfies the computational affordability requirements of both methods.

The choice of $\mathbf{v}(\mathbf{x},t)$ for the advection-propagation problem is as follows. Formally,

$$\mathbf{v}(\mathbf{x},t) = V\mathbf{e}_i \sin(\omega t)\sin(kx_j + r), \tag{26}$$

where V is a velocity amplitude, ω and k are fixed, and r and the direction indices i and j are time-dependent random variables in the following sense. The integers i and j (ranging from 1 to d) and the real number r are randomly selected at regular time intervals $t = n\pi/\omega$, $n = 1, 2, 3, \ldots$. These random selections, subject to the constraint $i \neq j$, change the orientation and the direction of spatial variation of the velocity field and introduce a random shift along the coordinate axis in that direction. These changes do not cause discontinuous time derivatives of the velocity field because they are implemented only when the time-modulation factor $\sin(\omega t)$ is zero.

The velocity field specified by Eq. (26) is not isotropic, though it is invariant under permutation of Cartesian axis labels. This is not a concern in the weak perturbation limit because the longitudinal perturbations dominate in this limit. Numerical results indicate that scalings beyond this limit are likewise unaffected.

An analog of Eq. (26) for the fixed heterogeneous medium can be formed by removing the orientation vector $\mathbf{e}_i$. In this case, the analysis of D is complicated. For simplicity, j is constrained to the transverse direction(s) for the heterogeneous case. This breaks the invariance to axis permutations that is obeyed in the advected case. Again, the scalings do not appear to be affected.

To apply the analysis of the weak perturbation limit to the exemplar perturbing fields, the diffusivity D defined in Sec. III B is evaluated for these perturbing fields in the Appendix. For the advection-propagation problem, the substitution of D, given by Eq. (A2), into Eq. (23) gives

$$\frac{u_T}{\lambda} - 1 = \frac{A}{[d(d-1)\phi_\lambda]^{2/3}} \left(\frac{1-\cos(k\xi)}{k\xi}\right)^{2/3} \left(\frac{v'}{\lambda}\right)^{4/3}, \tag{27}$$

where numerical coefficients are subsumed into A and ϕ_λ denotes the "phase velocity" $\frac{\omega/k}{\lambda}$.

The analogous result for heterogeneous propagation is obtained by replacing the term $d(d-1)$ by $(d-1)$ in Eq. (27). The difference between the two results is solely a reflection of the different formulations of the perturbing field in the two cases because, as explained in Sec. III B, the two propagation processes become equivalent in the weak fluctuation limit. Thus the comparison between the two propagation processes becomes, in this limit, a comparison between two different perturbation fields. For v'/λ not small, the two processes are mechanistically distinct.

Equation (27) and its analog for the case of hetero-

geneous propagation express u_T/λ in terms of v'/λ and ϕ_λ. On physical grounds, a more obvious parametrization would be in terms of v'/λ and $\phi_v = \frac{\omega/k}{v'}$. Variation of v'/λ for fixed ϕ_v corresponds to variation of the propagation rate for fixed flow parameters. In contrast, variation of v'/λ for fixed ϕ_λ implies simultaneous variation of the propagation rate and the frequency parameter ω.

Parametrization in terms of ϕ_v modifies the dependence on v'/λ in Eq. (27), giving instead the $\frac{2}{3}$-power dependence derived earlier for the case of autonomous perturbations. This reflects an artifact of the exemplar perturbing field, namely, the lack of spatial variation of $\mathbf{v}$ in the direction of the velocity vector. The characteristic time scale for variation of w is therefore determined not by spatial variation of $\mathbf{v}$ but by its temporal variation, governed by the frequency ω. In this regard, the exemplar case is analogous to the case of autonomous perturbations, with $1/\omega$ corresponding to the time scale τ_v.

The parametrization involving ϕ_λ is adopted because this parameter has been shown to govern the response of the interface to perturbations in a related class of deterministic flows [27]. It is of interest to examine dependences on ϕ_λ for the class of flows represented by Eq. (26), which involve randomization.

The results of a numerical study parametrized in this manner are shown in Fig. 2. The numerical method is outlined in Sec. IV B, and comparisons to the analysis of Sec. III are discussed in Sec. IV C.

B. Numerical method

The exemplar perturbing field, Eq. (26), has been formulated so that it is computationally tractable using both the front-tracking technique and the field-equation technique. The front-tracking technique is formulated for computational efficiency in the regime $v'/\lambda \ll 1$. An efficient algorithm is needed for $v'/\lambda \ll 1$ because in this regime, the distance over which the front must propagate to achieve relaxation of initial transients is large.

Namely, the relaxation distance is $u_T\tau_d$, where for

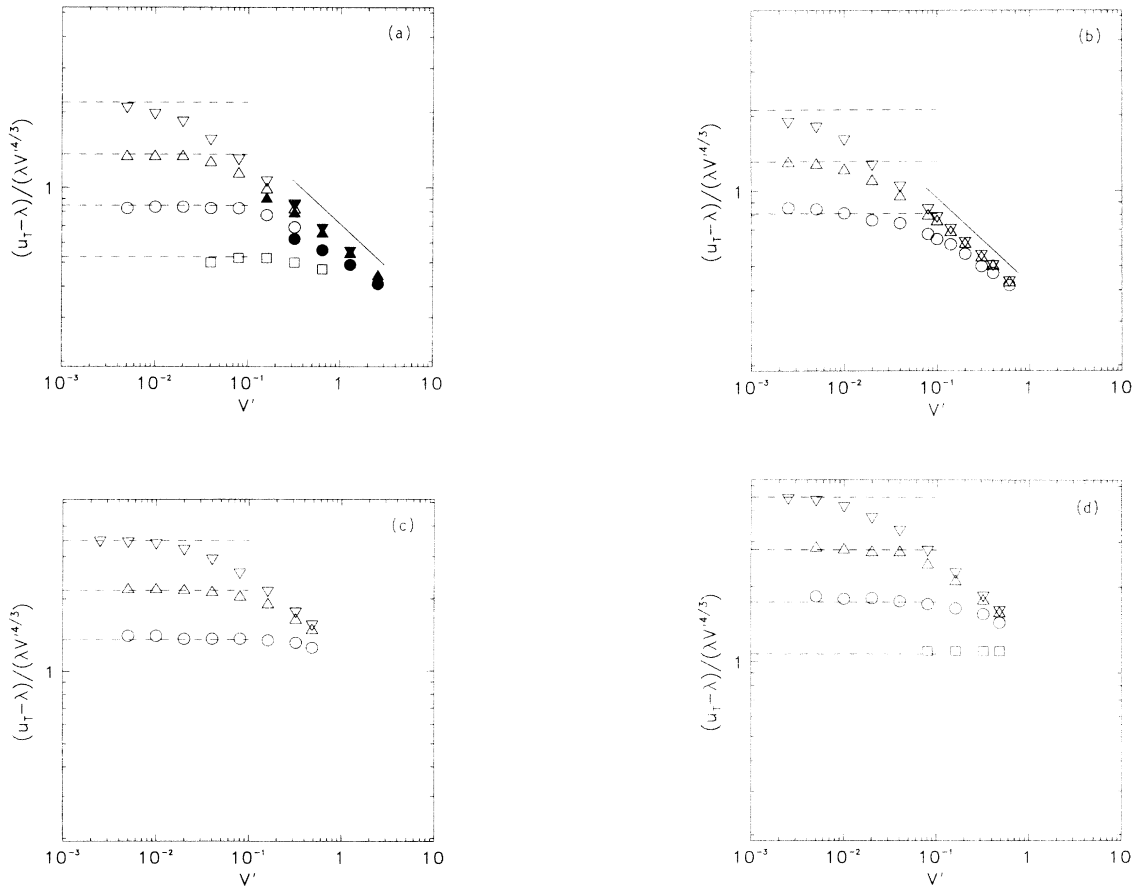

FIG. 2. Scaled passage rate versus scaled perturbation amplitude $V' = v'/\lambda$, computed for the exemplar class of perturbing fields with normalized phase velocity $\phi_\lambda = 1/4$ ($\triangledown$), 1/2 ($\triangle$), 1 ($\bigcirc$), 2 ($\square$). Open symbols, front-tracking computations, filled symbols, field-equation computations, dashed lines, model results in the weak fluctuation limit based on a d-dependent fitted coefficient, as discussed in the text. Advection-propagation problem for (a) $d = 2$ and (b) $d = 3$. Heterogeneous propagation problem for (c) $d = 2$ and (d) $d = 3$. For the advection-propagation problem, solid lines correspond to the linear dependence of passage rate on perturbation amplitude obtained in the strong perturbation limit.

$v'/\lambda \ll 1$, $u_T \approx \lambda$ and τ_d is given by Eq. (10). For the exemplar perturbing field, Eq. (A2) indicates that $D \sim v'^2/\omega$. Therefore the relaxation distance is of order $(k\xi)^{4/3}\phi_\lambda^{1/3}k^{-1}(v'/\lambda)^{-2/3}$, which greatly exceeds the flow length scale $1/k$ for $v'/\lambda \ll 1$ (unless $k\xi$ vanishes at a sufficient rate as v'/λ decreases, a possibility that is ruled out by subsequent numerical results).

The front-tracking technique applied here was used previously [9], but was described only briefly, so the numerical algorithm is described in detail for the case $d = 3$. The front is assumed to be a single-valued function $H(x_i, x_j)$ of transverse coordinates (x_i, x_j), where H is the front location in the longitudinal coordinate. [The indices i and j here represent particular transverse directions, in constrast to their meaning in Eq. (26).] Overall propagation is in the direction of increasing H. The front moves normal to itself due to advection and propagation (or propagation only, for the heterogeneous propagation problem). This normal motion is projected onto the longitudinal coordinate, neglecting the transverse component of the motion. This simplification is valid in the weak perturbation limit (see Sec. III B). Based on these considerations, Eq. (1) yields

$$\frac{\partial H}{\partial t} = \lambda\sqrt{1 + (\nabla H)^2} + v_\parallel \tag{28}$$

for the advection-propagation problem and an analogous expression for the heterogeneous propagation problem.

For the exemplar perturbation field, length is scaled by $2\pi/k$ and velocity is scaled by λ. The front, which is periodic in x_i and x_j with period unity in these units, is simulated on a transverse unit square with grid spacing 1/64. Discretized front locations are labeled $H(i,j)$. The average H_a of H at the four points $(i,j), (i+1,j), (i,j+1)$, and $(i+1,j+1)$ is assigned a nominal coordinate $(i+\frac{1}{2}, j+\frac{1}{2})$. The slope of the surface at each (i,j) is determined from these averaged heights, thus incorporating a smoothing effect into the gradient determination. The gradient squared is

$$[\nabla H(i,j)]^2 = \frac{[H_a(i+\frac{1}{2}, j+\frac{1}{2}) - H_a(i-\frac{1}{2}, j-\frac{1}{2})]^2}{\Delta^2} + \frac{[H_a(i-\frac{1}{2}, j+\frac{1}{2}) - H_a(i+\frac{1}{2}, j-\frac{1}{2})]^2}{\Delta^2}, \tag{29}$$

where Δ is the diagonal grid spacing. There are two exceptions to this relation, when $H(i,j)$ is a local maximum $H(i,j) > H_a(i \pm \frac{1}{2}, j \pm \frac{1}{2})$ or a local minimum $H(i,j) < H_a(i \pm \frac{1}{2}, j \pm \frac{1}{2})$.

For $H(i,j) > H_a(i \pm \frac{1}{2}, j \pm \frac{1}{2})$, the gradient is set to zero. In this case the propagation is taken to be the longitudinally directed at the nominal unit rate. Due to nonzero gradients at nearby nodes, the advancement there will be at a rate larger than unity, so the front location at those nodes may catch up with the local maximum. If the gradient were not set to zero at local maxima, then these points would continue to exceed the advancement rate of their neighbors and the surface would suffer increasing distortion, an artifact of spatial discretization.

At local minima, corresponding to the condition $H(i,j) < H_a(i \pm \frac{1}{2}, j \pm \frac{1}{2})$, one-sided estimates of the square of the slope are computed in each direction along a given diagonal, and the larger of the two is used. For example, the larger of $[H_a(i+\frac{1}{2}, j+\frac{1}{2}) - H(i,j)]^2/(\Delta/2)^2$ and $[H_a(i-\frac{1}{2}, j-\frac{1}{2}) - H(i,j)]^2/(\Delta/2)^2$ is taken to be the squared slope along the corresponding diagonal. A minimum location may correspond to a cusp in the surface. The one-sided estimates will yield the maximum advancement in the vicinity of a cusp. This reflects the fact that the most rapid advance in the vicinity of a cusp corresponds to the physical branch of the multiple-valued solution for front evolution. In contrast, use of central differencing across a cusp would give a lower, possibly zero, rate of advance, causing an unphysical prolongation of the cusp feature.

For the advection-propagation problem the front is advanced with the specified advection velocity and then the normal propagation at rate unity is determined from a predictor-corrector scheme. For the heterogeneous propagation problem the local propagation rate is incorporated into the predictor-corrector scheme.

This algorithm exploits the near alignment of the normal vector with the longitudinal direction in order to achieve the efficiency needed for affordable computation in the weak perturbation limit. Consequently, its validity for v'/λ of order unity is problematic. Therefore, the approach that is taken is to check representative front-tracking results for larger v'/λ by comparing them to results obtained using the field-equation technique, which does not involve weak perturbation approximations. This check is performed for the advection-propagation problem in two dimensions, for three choices of ϕ_λ.

The field-equation technique has been described previously [26], so only a brief summary is presented. For the two-dimensional advection-propagation problem, the equation

$$\frac{\partial G}{\partial t} + \mathbf{v} \cdot \nabla G = \lambda|\nabla G| + \epsilon\nabla^2 G \tag{30}$$

is solved numerically on a 64^2 grid with the initial condition $G(\mathbf{x}) = x_\parallel$, where $x_\parallel$ is the longitudinal component of $\mathbf{x}$. The boundary conditions are periodic in the transverse direction and jump periodic in the longitudinal direction, constraining the functional form of the velocity field $\mathbf{v}(\mathbf{x}, t)$ that can be simulated [hence the considerations leading to Eq. (26)]. For $\epsilon = 0$, each isopleth $G(\mathbf{x}, t) = G_0$ is convected by the field $\mathbf{v}(\mathbf{x}, t)$ and propagates in the direction of decreasing G at speed λ along the local normal. Each isopleth is thus a realization of the advection-propagation problem.

The dissipation factor ϵ is assigned a value large enough to suppress instabilities arising from spatial and temporal discretization. The grid spacing and time step are chosen so that instabilities can be suppressed at a value of ϵ small enough so that the dissipation term does not cause large systematic errors. For the computations reported here, $\epsilon = 0.004$.

The systematic errors associated with this technique

are those typically arising in the finite-difference solution of convection problems. For given spatial and temporal resolution, these errors depend primarily on the typical magnitude of the velocity field being simulated, which in this instance is u_T. Therefore the relative error of results for $u_T - \lambda$ increases as this difference becomes small compared to u_T, which occurs for small v'/λ.

For either technique, statistical precision of the computed value of u_T is determined by the time duration of the simulation. The precision of the computed results is indicated by the deviations of individual data points in Fig. 2 from a smooth dependence on v'/λ.

C. Results and comparisons

Figure 2 shows the computed v'/λ dependence of u_T, scaled so that 4/3-power dependence of $u_T - \lambda$ on v'/λ corresponds to a plateau on the plots. In these scaled log-log plots, linear dependence on v'/λ corresponds to linear falloff with slope $-1/3$.

For the advection-propagation problem in two dimensions, the extrapolation of front-tracking results to large v'/λ is consistent with field-equation results in that regime. Discrepancies are apparent at the smallest v'/λ values for which both techniques were used. These discrepancies evidently reflect systematic errors in the field-equation technique rather than the failure of weak perturbation approximations in the front-tracking technique, because the techniques are in best agreement at higher v'/λ values for which the field-equation technique becomes increasingly reliable (see Sec. IV B). This indicates that the validity of the front-tracking technique, at least for the purpose of computing u_T, extends to v'/λ of order unity.

In all cases, the computed results indicate decreasing sensitivity to ϕ_λ as v'/λ increases. This implies a tendency for the ratio u_T/v' to become insensitive to details of interface geometry in the strong perturbation limit. The generality of this inference cannot be determined from this limited sensitivity study. (Note that the range of v'/λ for the heterogeneous propagation problem is bounded because $\lambda+v$ must be non-negative, requiring $V \leq \lambda$ and thus $v'/\lambda \leq 1/2$.)

Figure 2 indicates that the exemplar perturbing field conforms to the predicted dependences on v'/λ in both the weak and strong perturbation limits. This is the first explicit demonstration of both limiting behaviors for a given exemplar case. In Sec. III B it was shown that the two-point model accounts for the scaling in the weak perturbation limit and that dimensional reasoning accounts for the scaling in the strong perturbation limit. An important goal for combustion and other physical applications is to formulate a mechanistically based model that captures both limiting behaviors and transition between them [25]. The results shown in Fig. 2 provide a quantitative benchmark for such a model.

Dashed lines in Fig. 2 are obtained from Eq. (27) based on the assumption that $k\xi$ may depend on d but not on v'/λ or ϕ_λ. Therefore the term involving $k\xi$ in Eq. (27) is subsumed in the coefficient A. The model results indicated by the dashed lines correspond to numerical values $A = 1.35$ for $d = 2$ and $A = 2.7$ for $d = 3$, chosen to fit the simulation results.

Comparison of the model and the simulations indicates the validity of the assumption that $k\xi$ is independent of v'/λ and ϕ_λ. The independence of v'/λ is implied by convergence of each data set to a plateau as v'/λ decreases, indicating that the $\frac{4}{3}$-power dependence on v'/λ in Eq. (27) fully accounts for the dependence of u_T/λ on v'/λ in the weak perturbation limit.

The results also indicate that $k\xi$ is insensitive to structural details of the perturbing field. This insensitivity is indicated first, by the confirmation of the $-\frac{2}{3}$-power dependence on the parameter ϕ_λ that governs temporal response to perturbations and second, by the good agreement that is obtained using the same value of A for the advection-propagation and heterogeneous propagation problems, which are formulated to have distinct spatial structures (see Sec. IV A). It cannot be determined from these results whether $k\xi$ is independent of d because other quantities with unknown d dependences have been subsumed into the parameter A.

It is inferred that the interface length scale ξ is proportional to the perturbation length scale $1/k$ insofar as the present comparisons can assess the relationship between these scales. This result mitigates a key limitation of the analysis, the inability to analyze systematically, or even to define precisely, the scale ξ. The result is consistent with, and generalizes, the previous observation that ϕ_λ parametrizes the response of the interface to perturbations in a restricted class of deterministic flows [27].

The utility of the present analysis hinges largely on the hypothesis that the ratio L/ξ in Eq. (24) has a simple dependence on the structure of the perturbing field. The present results support this hypothesis, but do not conclusively establish its correctness. In this regard, further numerical as well as analytical studies would be beneficial.

V. EXTENSION TO SELF-SIMILAR PERTURBATIONS

Though there is no formal restriction on the bandwidth of the perturbing field in Sec. III, the underlying physical assumptions are not *a priori* valid in the case of broadband perturbations. The analysis in Sec. III involves only one length scale L and one velocity scale v'. Here the case of a self-similar broadband perturbing field is analyzed using a variant of the scaling technique applied by Pocheau to turbulent flame propagation [24].

For this purpose, Eq. (18) is modified in a way that does not affect the leading-order parameter dependences but leads to a scale-invariant result that introduces higher-order corrections. The modification is based on the observation that the sweeping speed is taken to be λ in Eq. (15), but it is (slightly) more accurate to set the sweeping speed equal to the mean passage rate u_T. On this basis, λ is replaced by u_T in Eq. (17). Proceeding as in the derivation of Eq. (18), the relation

$$\frac{u_T}{\lambda} - 1 = A\left(\frac{v'^2}{\lambda u_T}\right)^{2/3} \tag{31}$$

is obtained, where L/ξ has been assumed constant and is therefore subsumed, along with other numerical factors, into the coefficient A.

Equation (31) is treated as a recursive equation determining the effective passage rate $u_{T,i}$, corresponding to a length scale indexed by i, in terms of the effective passage rate $u_{T,i-1}$ for the next smaller length scale (index $i-1$) and the level-i component v_i' of the root-mean-square fluctuation of the perturbing field. Here successive increments of i represent geometrically increasing length scales. This interpretation of Eq. (31) is implemented by the substitutions $u_T \to u_{T,i}$, $\lambda \to u_{T,i-1}$, and $v' \to v_i'$. Writing $u_{T,i} - u_{T,i-1} = du_{T,i}/di$ and rearranging terms, the difference equation

$$\frac{du_{T,i}}{di} = A\frac{v_i'^{4/3}u_{T,i-1}^{1/3}}{u_{T,i}^{2/3}} \tag{32}$$

is obtained. In the weak perturbation regime, $u_{T,i}$ is a slowly varying function of i, so $u_{T,i-1}$ can be replaced by $u_{T,i}$ on the right-hand side. With these substitutions, integration of Eq. (32) from $i = 0$ to the maximum level $i = I$ gives

$$u_{T,I}^{4/3} = u_{T,0}^{4/3} + \frac{4A}{3}\int_0^I v_i'^{4/3}\,di. \tag{33}$$

In inertial-range turbulence (but not limited to that case), the dominant contribution to velocity fluctuations is from the largest length scale, corresponding to level I. In other words, $v_I'^{4/3}$ is the dominant contribution to the integral and is approximately equal to $v'^{4/3}$. Noting also that $u_{T,0}$ corresponds to the propagation speed λ and $u_{T,I}$ corresponds to the mean passage rate u_T, the result

$$u_T^{4/3} = \lambda^{4/3} + \frac{4A}{3}v'^{4/3} \tag{34}$$

is obtained. This expression belongs to the class of scale-invariant relations identified by Pocheau [24].

From Eq. (34), the leading-order dependence of $u_T - \lambda$ on v'/λ derived in Sec. III B is recovered. Equation (34) introduces higher-order corrections to this dependence. Their significance cannot be assessed because higher-order corrections to the narrow-band result have not been analyzed.

It is noted in Sec. III B that the characteristic time τ_d governing the propagation process is much longer than the time for the front to sweep forward one correlation length in the weak perturbation limit. Accordingly, the longitudinal distance that must be traversed for relaxation to statistically steady propagation greatly exceeds the correlation length. In turbulent flow, the correlation length is typically of the order of the size of the flow domain, so transient effects must be considered in the weak perturbation limit. Here the transient propagation of an initially planar front is analyzed.

Quantitative analysis of transient effects in a finite domain requires incorporation of inertial-range turbulence scaling. In particular, the velocity fluctuations v_l' corresponding to length scale l scale as $v_l' \sim (l/L_I)^{1/3}v'$ for $L_K < l < L_I$ [18]. Here L_I denotes the "integral scale" (i.e., correlation length) of the flow and L_K denotes the Kolmogorov microscale representing the size of the smallest eddies not dominated by viscous damping.

Broadband perturbations are obtained in the strong turbulence regime $L_I \gg L_K$. Adopting the usual approach for analyzing scalings in this regime [18], perturbations corresponding to a typical length scale l in this range are considered. The effect of these perturbations on transient propagation is determined by applying the narrow-band analysis. Incorporation of the turbulence scaling determines the l dependence of the result, leading to identification of the range of l values subject to transient effects.

Transient propagation in the weak perturbation regime is analyzed using the two-point model. The initially planar front corresponds to $g = 0$. Because the random forcing and decay terms of Eq. (6) balance on a time scale τ_d, the decay term is negligible during the transient interval $0 < t \ll \tau_d$. g therefore evolves during the transient as a random walk. Substitution of the random walk scaling $\langle g^2\rangle \sim Dt$ into Eq. (9), with D given by Eq. (17) and L/ξ assumed constant, gives $[u_T(x) - \lambda]/\lambda \sim (v'/\lambda)^2 x/L$ for propagation a distance x, where $L \ll x \ll \lambda\tau_d$. Here $u_T(x)$ is the transient passage rate $\frac{x}{t(x)}$, where $t(x)$ is the transit time over a distance x and $\lambda\tau_d$ is the relaxation distance based on $u_T \approx \lambda$.

This result is for the case of narrow-band perturbations with correlation length L. It is applied to size-l perturbations within a broadband flow by the substitutions $u_T \to u_{T,l}$, $v' \to v_l'$, and $L \to l$. For x equal to the turbulence integral scale L_I, this gives

$$\frac{u_{T,l}(L_I) - \lambda}{\lambda} \sim \left(\frac{v_l'}{\lambda}\right)^2\frac{L_I}{l} \sim \left(\frac{v'}{\lambda}\right)^2\left(\frac{L_I}{l}\right)^{1/3}. \tag{35}$$

The rightmost expression is obtained by substituting the turbulence scaling relation for v_l'.

This result is valid for length scales l such that $\lambda\tau_l \geq L_I$, where $\tau_l \sim (\lambda/v_l')^{2/3}l/\lambda$ based on application of Eq. (19) to size-l perturbations. Substituting the turbulence scaling relation for v_l', this implies that length scales $l \geq (v'/\lambda)^{6/7}L_I \equiv l^*$ are governed by the transient analysis, but smaller scales are governed by the steady-state relation $[u_{T,l}(L_I) - \lambda]/\lambda \sim (v_l'/\lambda)^{4/3}$. Within the range $l < l^*$, $u_{T,l}(L_I)$ is largest for $l = l^*$. According to Eq. (35), $u_{T,l}(L_I)$ is a decreasing function of l in the range $l > l^*$ corresponding to transient propagation. This identifies l^* as the dominant length scale, so finally,

$$\frac{u_T(L_I) - \lambda}{\lambda} \sim \frac{u_{T,l^*}(L_I) - \lambda}{\lambda} \sim \left(\frac{v'}{\lambda}\right)^{12/7}, \tag{36}$$

which follows either from Eq. (35) or from the steady-state relation evaluated at $l = l^*$. (Their agreement at $l = l^*$ is the matching condition for the transient and steady-state ranges of l.) Note, however, that this result applies only if $l^* > L_K$, where the dependence of L_K on the flow Reynolds number is given by the turbulence

scaling law $L_K \sim \mathrm{Re}^{-3/4} L_I$ [18]. Thus Eq. (36) is valid for $\mathrm{Re} > (\lambda/v')^{8/7}$, which should hold for most cases of interest. If this condition is not obeyed, then the transient analysis applies for all $l \geq L_K$, and the dominant length scale is $l = L_K$. Evaluation of Eq. (35) for $l = L_K$ then gives

$$\frac{u_T(L_I) - \lambda}{\lambda} \sim \mathrm{Re}^{1/4} \left(\frac{v'}{\lambda}\right)^2 . \tag{37}$$

Examples of propagation through a weak, broadband perturbation field are optical propagation through atmospheric turbulence and acoustic propagation through oceanic turbulence. (The broadband property arises because the power spectrum of refractive-index fluctuations reflects the power spectrum of turbulent velocity fluctuations that mix zones of differing refractive index.) The application of the results of this section to propagation in geophysical flows may require modifications to account for stratification and other factors that complicate the structure of these flows.

VI. DISCUSSION

Modeling and numerical simulation have been applied here to a class of interface propagation processes involving media that are randomly stirred or heterogeneous. The model involves transverse discretization but a continuum treatment of longitudinal evolution. A comparison of model predictions to numerical results supports this approach. In particular, the results support the predicted $\frac{4}{3}$-power dependence of $u_T - \lambda$ on v'/λ in the weak perturbation limit, previously obtained by dimensional analysis [9].

That analysis and the present formulation indicate that statistically steady interface propagation through a location-dependent (as opposed to autonomous) perturbation field is governed by a relaxation length scale $\lambda\tau_d$ that is much larger than the correlation length of the perturbing field in the weak perturbation limit. This slow relaxation, which underlies the $\frac{4}{3}$-power dependence, is a manifestation of a nonlinearity of geometrical origin in the governing equation. The physics underlying the slow relaxation was recognized previously in a different context [28].

The slow relaxation indicates the need for care in performing numerical simulations (and likewise, experiments and field observations) to ensure that transient effects are properly interpreted. In particular, for $v'/\lambda \ll 1$ it is found that the passage rate though self-similar flows governed by inertial-range turbulence scalings is governed by a microscale $l^* = (v'/\lambda)^{6/7} L_I$. Here l^* is the characteristic size of the largest eddies for which the relaxation length scale is less than the turbulence integral scale L_I. The identification of this microscale leads to a scaling law governing the mean passage rate through a turbulent flow of size L_I.

The two-point model formulated here provides a geometrical interpretation of the scaling properties underlying these results and extends the previous analysis by parametrizing the coefficient in the relation between the mean passage rate and the perturbation amplitude. The coefficient is found to involve a ratio of characteristic length scales of the perturbing field and the propagating interface. Numerical simulations indicate that this ratio depends only on spatial dimension. This conclusion should be regarded as tentative pending more extensive parametric studies.

The formulation of a physically valid extension of the analysis to strong perturbations is an open question. The numerical simulations reported here exhibit the linear dependence of u_T on v' that is expected in this regime based on dimensional considerations. The simulations capture the entire range of v'/λ dependence for a given class of perturbing fields, providing a benchmark for future efforts to extend the analysis beyond the weak perturbation regime.

ACKNOWLEDGMENTS

The authors thank F. A. Williams and V. Yakhot for helpful discussions. This research was supported by the Division of Engineering and Geosciences and the Division of Chemical Sciences, Office of Basic Energy Sciences, U.S. Department of Energy.

APPENDIX: PROPERTIES OF AN EXEMPLAR CLASS OF PROPAGATION PROCESSES

Properties of the advection-propagation problem with the velocity field given by Eq. (26) are derived. Results for the heterogeneous propagation problem defined in Sec. IV A are also presented; the derivations closely parallel those for the advection-propagation problem.

The mean-square fluctuation v'^2 is obtained by squaring Eq. (26) and noting that the ensemble average involves a time average of $\sin^2(\omega t)$ and a spatial average of $\sin^2(kx_j + r)$. Each of these averages contributes a factor $1/2$, giving $v'^2 = V^2/4$.

The diffusion coefficient D is evaluated based on Eq. (12). The simpler approximate expressions for D derived in Sec. III B are not used because they are based on an assumed rapid falloff of spatial correlations, which is not valid for the exemplar class of processes. In any event, Eq. (12) is readily evaluated for these processes.

For the flow under consideration, it is important to recognize that the averages indicated in Eq. (12) are ensemble averages. An individual realization of the flow does not obey strict time invariance due to the imposed time periodicity. To express the ensemble averages in terms of time averages, the velocity arguments $(h_1(0), 0)$ in Eq. (12) are replaced by $(h_1(t_0), t_0)$ and the lower limits of integration are set equal to t_0. The ensemble average now corresponds to a spatial average (implemented shortly) and a time average over t_0, implemented by inte-

grating the right-hand side of Eq. (12) over $0 \leq t_0 \leq \pi/\omega$ with normalization factor ω/π. The upper bound of each integral over t is set equal to π/ω, reflecting the random adjustments of the flow field at epochs $n\pi/\omega$. (These adjustments cause the time correlations to vanish if $t_0 < \pi/\omega < t$.)

Assuming that the longitudinal direction in the two-point model corresponds to a coordinate axis, a nonzero contribution to D is obtained only if direction i corresponds to that axis. Otherwise, v_1 in Eq. (12) is zero everywhere. Assuming also that the direction represented by the separation $x_2 - x_1$ in the two-point model corresponds to a coordinate axis, j must correspond to the same axis, or else $v_1(h_2(t),t) = v_1(h_1(t),t)$ and the two integrals in Eq. (12) cancel. Therefore Eq. (12) is evaluated by conditioning on particular values of i and j and multiplying the result by the probability $1/[d(d-1)]$ of obtaining a particular pair of values.

Based on these considerations, substitution of Eq. (26) into Eq. (12) gives

$$D = \frac{2V^2}{d(d-1)}\frac{\omega}{\pi}[\langle \sin^2(r)\rangle - \langle \sin(r)\sin(k\xi + r)\rangle] \times \int_0^{\pi/\omega} dt_0 \sin(\omega t_0) \int_{t_0}^{\pi/\omega} dt \sin(\omega t), \quad \text{(A1)}$$

where the angular brackets now denote averages over the random variable r. Evaluation of the right-hand side of Eq. (A1) gives the result

$$D = \frac{8v'^2}{\pi\omega d(d-1)}[1 - \cos(k\xi)] \quad \text{(A2)}$$

for the advection-propagation problem.

For the heterogeneous propagation problem as formulated in Sec. IV A, the analysis is identical except that the probability factor $1/[d(d-1)]$ is replaced by $1/(d-1)$ because there is no random selection of the orientation index i. Therefore D for this problem is obtained by multiplying the right-hand side of Eq. (A2) by d.

[1] D. Mollison, J. R. Stat. Soc. B **39**, 283 (1977).
[2] J. D. Murray, *Mathematical Biology* (Springer-Verlag, New York, 1989).
[3] *Random Fluctuations and Pattern Growth: Experiments and Models*, edited by H. E. Stanley and N. Ostrowsky (Kluwer, Dordrecht, 1988).
[4] J. C. Wierman, Ann. Prob. **10**, 509 (1982).
[5] S. Havlin and D. Ben-Avraham, Adv. Phys. **36**, 695 (1987).
[6] H. Kesten, Ann. Prob. **15**, 1231 (1987).
[7] S. Torquato, Lect. Appl. Math. **27**, 323 (1991).
[8] S. Torquato, Appl. Mech. Rev. **44**, 37 (1991).
[9] A. R. Kerstein and W. T. Ashurst, Phys. Rev. Lett. **68**, 934 (1992).
[10] H. G. E. Hentschel and F. Family, Phys. Rev. Lett. **66**, 1982 (1991).
[11] M. Kardar, G. Parisi, and Y.-C. Zhang, Phys. Rev. Lett. **56**, 889 (1986).
[12] J. G. Amar and F. Family, Phys. Rev. A **45**, 5378 (1992).
[13] F. A. Williams, *Combustion Theory*, 2nd ed. (Benjamin-Cummings, Menlo Park, CA, 1985).
[14] P. F. Worcester, B. D. Cornuelle, and R. C. Spindel, Rev. Geophys. Suppl. **29**, 557 (1991).
[15] A. R. Kerstein, Combust. Flame **69**, 95 (1987).
[16] M. Karweit, P. Blanc-Benon, D. Juvé, and G. Comte-Bellot, J. Acoust. Soc. Am. **89**, 52 (1991).
[17] R. Kubo, J. Math. Phys. **4**, 174 (1963).
[18] H. Tennekes and J. L. Lumley, *A First Course in Turbulence* (MIT Press, Cambridge, MA, 1972).
[19] V. S. L'vov, Phys. Rep. **207**, 1 (1991).
[20] C. W. Gardiner, *Handbook of Stochastic Methods*, 2nd ed. (Springer-Verlag, Berlin, 1990).
[21] C. Bender, F. Cooper, L. M. Simmons, Jr., P. Roy, and G. Kilcup, J. Stat. Phys. **64**, 395 (1991).
[22] V. Yakhot, Combust. Sci. Tech. **60**, 191 (1988).
[23] V. Yakhot, Combust. Sci. Tech. **62**, 127 (1988).
[24] A. Pocheau, Phys. Rev. E **49**, 1109 (1994).
[25] A. Liñán and F. A. Williams, *Fundamental Aspects of Combustion* (Oxford, New York, 1993).
[26] A. R. Kerstein, W. T. Ashurst, and F. A. Williams, Phys. Rev. A **37**, 2728 (1988).
[27] W. T. Ashurst, G. I. Sivashinsky, and V. Yakhot, Combust. Sci. Tech. **62**, 273 (1988).
[28] V. A. Kulkarny and B. S. White, Phys. Fluids **25**, 1770 (1982).